Published in final edited form as:
Mol Cancer Ther. 2010 August ; 9(8): 2354–2364. doi:10.1158/1535-7163.MCT-10-0207.

Immune Competency of a *Hairless* Mouse Strain for Improved Preclinical Studies in Genetically-Engineered Mice

Beverly S. Schaffer[1,#], **Marcia H. Grayson**[2,#], **Joy M. Wortham**[1], **Courtney B. Kubicek**[1], **Amanda T. McCleish**[1], **Suresh I. Prajapati**[1], **Laura D. Nelon**[1], **Michelle M. Brady**[1], **Inkyung Jung**[3], **Tohru Hosoyama**[1], **Leslea M. Sarro**[4], **Martha A. Hanes**[4], **Brian P. Rubin**[5], **Joel E. Michalek**[2,3], **Charles B. Clifford**[6], **Anthony J. Infante**[2,¥], and **Charles Keller**[1,7,*,¥]

[1] Greehey Children's Cancer Research Institute, University of Texas Health Science Center, San Antonio, TX 78229 USA

[2] Department of Pediatrics, University of Texas Health Science Center, San Antonio, TX 78229 USA

[3] Department of Epidemiology & Biostatistics, University of Texas Health Science Center, San Antonio, TX 78229 USA

[4] Department of Laboratory Animal Resources, University of Texas Health Science Center, San Antonio, TX 78229 USA

[5] Department of Anatomic Pathology, Cleveland Clinic, Taussig Cancer Center and the Lerner Research Institute, Cleveland, OH, USA

[6] Pathology and Technical Services, Charles River Laboratories, Wilmington, MA, USA

[7] Department of Cellular & Structural Biology, University of Texas Health Science Center, San Antonio, TX 78229 USA

Abstract

Genetically-engineered mouse models (GEMMs) of cancer are of increasing value to preclinical therapeutics. Optical imaging is a cost-effective method of assessing deep-seated tumor growth in GEMMs whose tumors can be encoded to express luminescent or fluorescent reporters, although reporter signal attenuation would be improved if animals were fur-free. In this study, we sought to determine whether hereditable furlessness resulting from a hypomorphic mutation in the *Hairless* gene would or would not also affect immune competence. By assessment of humoral and cellular immunity of the SKH1 mouse line bearing the hypomorphic *Hairless* mutation, we determined that blood counts, immunoglobulin levels, and CD4+ and CD8+ T cells were comparable between SKH1 and the C57Bl/6 strain. On examination of T cell subsets, statistically significant differences in naïve T cells (1.7 vs. 3.4×10^5 cells/spleen in SKH1 vs. C57Bl/6, p=0.008) and memory T cells (1.4 vs. 0.13×10^6 cells/spleen in SKH1 vs. C57Bl/6, p=0.008) were detected. However, the numerical differences did not result in altered T cell functional response to antigen re-challenge (keyhole limpet hemocyanin) in a lymph node cell *in vitro* proliferative assay. Furthermore, interbreeding the SKH1 mouse line to a rhabdomyosarcoma GEMM demonstrated

[*]corresponding author current address: Pape' Family Pediatric Research Institute, Department of Pediatrics, Oregon Health & Science University, 3181 S.W. Sam Jackson Park Road, Mail Code: L321, Portland, OR 97239-3098, Tel (503) 494-1210, Fax (503) 418-5044, keller@ohsu.edu.
[#,¥]contributed equally

All animal procedures were conducted in accordance with the Guidelines for Care and Use of Laboratory Animals and were approved by the Institutional Animal Care and Use Committee (IACUC) at the University of Texas Health Science Center at San Antonio (UTHSCSA).

preserved anti-tumor responses of CD56+ Natural Killer cells and CD163+ macrophages, without any differences in tumor pathology. The fur-free GEMM was also especially amenable to multiplex optical imaging. Thus, SKH1 represents an immune competent, fur-free mouse strain which may be of use for interbreeding to other genetically-engineered mouse models of cancer for improved preclinical studies.

Keywords

Hairless; SKH1; small animal imaging; rhabdomyosarcoma

Introduction

The mouse strain SKH1 carries an autosomal recessive hypomorphic mutation called *hr* in the gene *Hairless* (*Hr*) (1). This mutation is caused by a proviral insertion of the murine leukemia virus at the *Hr* locus (Fig. 1) (1). These mice undergo hair loss before weaning, a feature that could dramatically improve preclinical therapeutic investigation for genetically-engineered mouse models (GEMMs) of cancer. Specifically, GEMMs can be bred to the SKH1 strain in order to achieve furlessness, a feature which improves serial optical imaging of reporter genes and contrast agents in live animals (2). In transgenic mouse models of human disease, tumors or tissues are often genetically engineered to express luciferase or fluorescent proteins as optically-detectable reporters to determine the health, proliferation or migration (metastasis) of the cell population or tissue of interest. When wild-type mice are imaged, fur reduces luminescent and fluorescent reporter gene signal by more than 10 fold (3). Because even skin alone can reduce optical signal by 90% (4), the detection of small tumors or metastases using optical imaging is often quite challenging. Mice without fur would allow better imaging; however, for preclinical models to be physiologically accurate to human disease, fur-free GEMMs must also be immune competent.

The *Hr* gene encodes the protein Hr, which is highly expressed in the skin and brain and acts as a transcriptional co-repressor for multiple nuclear receptors, including thyroid hormone receptor, retinoic acid receptor, and the vitamin D receptor (5). The absence of the repressor protein HR in *hr* mice alters transcription of gene products that function in keratinocyte differentiation (5). In addition to changes in hair and skin development, mutations which affect keratinocyte gene expression may alter thymus development and cell mediated immunity, as dramatically illustrated by the homozygous nude phenotype due to disruption of *Foxn1* (6). Thus, mutations in the *Hr* gene have the potential to seriously impact immunological function, which underlies the purpose of our study evaluating immune function of the SKH1 mouse line.

First described by Brooke in 1926 (7), the homozygous SKH1 mouse line has been maintained in commercial breeding facilities without immunological precautions for years if not decades (CB Clifford, personal communications). This apparent immune competence may be in part because homozygous SKH1 mice still produce *Hr* transcript at ~5 % of normal levels (8), despite an insertion of murine leukemia virus (MuLV) *pmv*43 in exon 6 of *Hr* (1). *pmv*43 itself is believed to result from a recombination of xenotropic and polytropic classes of endogenous murine leukemia virus based upon restriction mapping (9,10). Humans are also known to carry mutations of the *HR* gene and have been reported to have skin and hair phenotypes ((OMIM 602302) and reference (11)), yet no associations with immunodeficiency or non-skin cancer predisposition have been made. Therefore, the goal of this study was to ascertain the immunological differences, if any, between mice homozygous for the autosomal recessive *Hr* mutation, SKH1, and a control C57Bl/6 mice line to ascertain whether the SKH1 mouse line can be used for preclinical therapeutic models in

GEMMs. Our assessment of humoral and cellular immune competence revealed relatively little functional immunological differences for the SKH1 strain in comparison to C57Bl/6.

Materials and Methods

Mice

All animal procedures were conducted in accordance with the Guidelines for Care and Use of Laboratory Animals and were approved by the Institutional Animal Care and Use Committee (IACUC) at the University of Texas Health Science Center at San Antonio (UTHSCSA). The SKH1 strain mice carrying the homozygous *Hairless* (*Hr*) mutation *hr* (also called *Hairless*$^{hr/hr}$ or *Hairless*$^{SKH1/SKH1}$) and the comparison C57Bl/6 control mice were purchased from Charles River Laboratories (catalog numbers SKH1:313 and C57Bl/6:027, respectively; CRL, Wilmington, MA). For all studies, 8–12 week old female mice were used unless otherwise specified. Tissues were harvested at necropsy following euthanasia under approved methods. The Pax3:Fkhr alveolar rhabdomyosarcoma mouse model used for transgenic experiments was previously described (3,12–14). PCR genotyping for the *Hr* mutation was performed using primers am05 (viral LTR) 5′-GCGTTACTGCAGCTAGCTTG-3′, am06 (*Hr* exon 6) 5′-TGTAGCCTGTGGTCGCATAG-3′, and am07 (*Hr* intron 6) 5′-CTCCTGTTTGCTTGGTCATC-3′ which produce a 350 base pair (bp) product for the wildtype allele and a 250 bp product for the SKH1 mutant allele. For tumor-bearing animals, tumor dimensions were measured with digital calipers and the volume was calculated from the formula $\pi/6 \times \text{length} \times \text{width} \times \text{height}$.

Complete blood counts

At the academic site, complete blood counts were performed on a VetScan HM2™ Hematology System (Abaxis, Union City, CA). Six mice (3 males and 3 females) ages 160–200 days were evaluated per strain. At the commercial site, complete blood counts were performed on a Hemavet 950 Veterinary Hematology Analyzer (Drew Scientific, Dallas, TX). Five SKH1 mice (sexes not specified) ages 180–240 days and 68 C57Bl/6 mice (34 males and 34 females) ages 56–70 days were evaluated. Statistical analysis was performed with the Wilcoxon rank-sum test.

Immunizations

Animals were immunized with a 1:1 emulsion of keyhole limpet hemocyanin (KLH; Sigma-Aldrich, St Louis, MO) in complete Freund's adjuvant. Animals received 25μg of KLH subcutaneously at the base of the tail. For some groups of mice, draining lymph nodes were collected after seven days and cell suspensions made by mechanical disruption and passage through a mesh screen for measurement of cellular responses. Other groups of mice were bled one week after immunization and then immunized thirty days after primary immunization with 5μg KLH in solution intraperitoneally. One week after secondary immunization, mice were bled again.

Immunoglobulin and antibody measurements

Serum IgM was measured using a commercial colorimetric ELISA assay kit (Immuno-Tek, Zepto-Metrix Corp., Buffalo, NY). Quantification was by comparison to a standard curve supplied with the kit. Serum IgA was measured using a similar ELISA kit (Alpha Diagnostic International, San Antonio, TX). Specific anti-KLH antibody responses were analyzed using commercial solid phase ELISA kits detecting anti-KLH IgM (5 days post-immunization) and IgG (2 weeks post immunization) (Life Diagnostics, Inc., West Chester, PA). Quantification was by comparison to a standard curve using a reference serum supplied with

the kits. For each assay, 11 to 15 mice per strain were evaluated. Statistical analysis was performed using a two-sample t-test for each assay.

Immunophenotyping

Cell suspensions were made from spleen and thymus by mechanical disruption and passage through a mesh filter. Lymphocyte phenotyping was performed using the following directly conjugated monoclonal antibodies, all supplied by the same manufacturer (BD Biosciences, San Jose, CA): PE-Cy7 hamster anti-mouse CD3ε, APC-Cy7 rat anti-mouse CD4, PerCP-Cy5.5 rat anti-mouse CD8a, APC rat anti-mouse CD25, PE rat anti-mouse CD44, PE rat anti-mouse CD49b, R-PE rat anti-mouse CD62L. Labeled cells were analyzed using a BD FACSAria instrument (BD Biosciences) in the UTHSCSA core flow cytometry laboratory. Individual small lymphocytes were gated by forward (FSC) and side (SSC) light scatter by strategies as presented in Supplementary Figure S1A to F (in these examples, Figure 1A to C is for spleen and Figure S1D to F is for thymus). One sample each of unstained and single-color stained cells was used to set thresholds for populations of interest. The remaining samples were then analyzed for the indicated markers by multi-color staining. Figure S1B is a representative dot plot of CD3 T cell and CD19 B cell analysis of spleen, while Figure S1E shows an example of CD4 and CD8 single positive, double positive (DP) and double negative (DN) T cell populations in thymus. Figure S1C and Figure S1F illustrate the relationship of the subpopulations used to generate the data shown in the tables. For each assay, 5 mice per strain were evaluated. Statistical analysis was performed using the Wilcoxon rank-sum test.

Cellular immune responses

Lymph node cells from unimmunized mice were placed in 96-well plastic tissue culture plates and incubated with 0.02μg/ml phytohemagglutinin (PHA) for five days. Lymph node cells from KLH-immunized mice were incubated in 96 well plates containing titrated doses of KLH for seven days. Sixteen hours prior to harvest, cells were pulsed with 1μg tritiated thymidine (^{3}H-TdR). Cells were collected on glass fiber filters and ^{3}H-TdR incorporation measured by liquid scintillation spectrometry. For each assay, 4 to 5 mice per strain and 14–20 overall replicates were evaluated. KLH diluent (vehicle) was used as a negative control and anti-CD3 was used as a positive control. Statistical analysis was performed using a linear mixed effects model with random coefficients of intercept and treatment (capturing overall variations among mice and variations due to changes over different treatments). Correlation structure was assumed to be different for two groups. Log-transformation was used on ^{3}H-TdR values to make the data normally distributed. Delayed-type hypersensitivity assay.

C57Bl/6 (n=5) and SKH1 (n=5) mice were initially sensitized by a subcutaneous injection at the base of the tail with 25 μg of KLH in 50 μl of a 1:1 emulsion of PBS:Complete Freunds Adjuvant. Seven days later the mice were challenged with 5 μg of KLH in 10 μl PBS injected subcutaneously in the left ear or with 10 μl PBS injected subcutaneously in the right ear. Two days later the thickness of both ears were measured to determine the *in vivo* immune response of the Bl6 and SKH1.

Quantitative RT-PCR for Hairless

Total RNA was isolated from mouse tail tissue using Trizol (Invitrogen, Carlsbad, CA) according to the manufacturer's specifications. RNA was then purified using the RNeasy miniprep kit (Qiagen, Valencia, CA) with the optional DNAse I treatment step. Using the first strand cDNA synthesis kit (Fermentas, Glen Burnie, MD), single-stranded cDNA was generated from total RNA according to the manufacture's instruction. Real time PCR was performed on an ABI Prism 7500HT Fast Real-Time PCR System (PE Applied Biosystems,

Foster City, CA). Quantification of *Hr* expression was performed using SYBR Green PCR Master Mix (PE Applied Biosystems) and the forward primer th009 (exon 6) 5′-ACCACGGACTCTTCAACACC-3′and the reverse primer th010 (exon 7) 5′-GGAGACAAACTGGGTCAGGA-3′ to generate a 188 bp product predicted by NCBI sequence gi 531706. Expression of *glyceraldehyde 3-phosphate dehydrogenase* (*Gapdh*) was determined using ABI TaqMan Fast Universal PCR Master Mix, with forward primer 5′-TGCACCACCAACTGCTTAG-3′, reverse primer 5′-GGATGCAGGGATGATGTTC-3′, and probe 5′-6-FAM-CAGAAGACTGTGGATGGCCCTC-TAMRA-3′ and the level of mRNA expression of *Hr* was normalized to *Gapdh*. Statistical analysis was performed using a two-sample t-test.

Histopathology

Histology using hematoxylin and eosin and immunohistochemistry were performed as previously described (3). Because tumor heterogeneity and necrosis can bias quantitation of NK killer cells and macrophages, those cell populations were only quantitated in non-necrotic areas.

Multiplex live animal imaging

Optical imaging for this experiment was performed using the Xenogen IVIS® Spectrum system (Caliper – Xenogen, Alameda, CA, USA). For the imaging experiment in Figure 4, a mouse of the genotype *Myf6*$^{\text{ICNm/WT}}$ *Pax3*$^{\text{P3Fm/P3Fm}}$ *Trp53*$^{\text{F2-10/F2-10}}$ *Rosa26*$^{\text{Lusapm/WT}}$ *Hr* $^{\text{SKH1/SKH1}}$ bearing a lower limb tumor was injected intravenously via tail vein with 100 μl of 0.2 mM IR-820 (Sigma-Aldrich, St. Louis, MO) in PBS as previously described (2) and 100 μl of 2 nM MMPSense 680 (VisEn Medical, Inc., Woburn, MA). This mouse was imaged after 24 hours with camera settings at 1 sec exposure time, 4x4 binning, 12.6 cm field of view, and f/stop of 1/2. The data was acquired and analyzed using the manufacturer's Living Image 3.2© software. The animal was imaged using the same anesthesia protocol of 2% isoflurane in 100% oxygen at 2.5 liters per minute. Body temperature was maintained at 37°C by a heated stage. The images were acquired using epi-illumination at an excitation wavelength of 680 nm and an emission wavelength of 720 nm for MMPSense 680, and at an excitation wavelength of 710 nm and an emission wavelength of 820 nm for IR-820. After recovery on a heatpad, the mouse was injected intraperitoneally with 200 μl of 15mg/ml D-Luciferin (Firefly potassium salt). Ten minutes after injection, the mouse was imaged with aforementioned camera settings with noexcitation and open emission filter.

Results

Hairless SKH1 mice develop progressive, rostral-caudal alopecia

The proviral insertion site of *pmv*43 into exon 6 of *Hr* is well-defined (Fig. 1A), and thus the recessive SKH1 allele can be readily genotyped by PCR (Fig. 1B) (1). SKH1 mice express 8.5% of the normal full length *Hr* transcript (Fig. 1C). This reduction of the correct transcript is the result of aberrant splicing of the *Hr* gene caused by the provirus (8). Mice develop progressive alopecia that begins at the eyes, forelimbs and nose then proceeds caudally by 4 weeks of life (Fig. 1D). This rostro-caudal wave pattern is consistent with the wave pattern of hair follicle activity in mice and has been previously reported for this *hr* mutant of *Hr* (15,16). The commercially available SKH1 strain is considered 'outbred', since by SNP-based assays approximately 75% of loci are homozygous for one allele and because the colony is maintained by an outbred breeding scheme (CB Clifford, personal communications).

Blood counts are similar between SKH1 mice and C57Bl/6 mice

Because the commercially-available SKH1 mouse strain is considered outbred (having first been established from a colony at the Skin and Cancer Hospital of Temple University in 1986; CB Clifford, personal communications), we sought to perform a full immunological evaluation of this *Hairless*$^{SKH1/SKH1}$ mouse strain in its current outbred state (hereafter referred to as the SKH1 mouse line). As our control mouse line, we chose the C57Bl/6 (hereafter referred to as the B6 mouse line) because C57Bl/6 is most commonly used in murine immunological studies. We began our immunological analyses with complete blood counts conducted independently for mice housed at academic and commercial sites (Table 1 and Supplementary Table S1, respectively). Only at the academic site were leukocyte counts different between SKH1 and B6 mice, in that the percentage of lymphocytes was lower in SKH1 than B6 mice (70 vs. 83%, p=0.05), although absolute lymphocyte counts were not different between strains. No other statistically significant trends were seen in independently compared complete blood counts. All subsequent experimental data for the SKH1 and B6 were obtained at the academic site.

Humoral immunity of SKH1 mice is comparable to C57Bl/6 at baseline and after immunization

The next step of our evaluation was to examine humoral immunity. For immunoglobulins, baseline IgM levels were lower in SKH1 than B6 mice (Fig. 2A; 2.66 vs. 3.49 ng/ml, p<0.0001). Baseline serum IgG and IgA levels were not significantly different (Fig. 2B, C). CD19 positive B cells from the spleen were comparable between SKH1 and B6 mice. Following immunization with keyhole limpet hemocyanin (KLH) antigen, levels of anti-KLH IgM were lower in 5 day post-immunization for SKH1 mice when compared to B6 mice (Fig. 2E; 0.12 vs. 0.11ng/ml, p=0.02), consistent with decreased baseline IgM levels for SKH1 mice. However, 2 week post-immunization anti-KLH IgG levels were appropriately elevated and similar in B6 and SKH1 mice (Fig. 2F). Thus, humoral immunity was similar between SKH1 and B6 mice except for lower IgM (but not IgG) levels in SKH1 mice.

Alterations in T cell subset expression in SKH1 mice were not associated with functional defects

We evaluated T cell subset distribution in thymus and spleen using multiplex flow cytometry. In comparison to B6, numbers and percentages of the major thymocyte subsets CD4/CD8 double negative (DN), double positive (DP), and single positive CD4 and CD8 subsets were not significantly different in SKH1 mice (Fig. 3A). These results suggested that the effect of the *hr* mutation on epithelial cells does not disturb thymocyte differentiation.

In the peripheral lymphoid compartment, represented by the spleen, the number of CD3+ cells was mildly increased (Fig. 3B; 2.3 vs. 4.5×10^5 cells/spleen in SKH1 vs. B6 mice, p=0.02), while the major CD4 and CD8 subsets were decreased (Fig. 3B). This finding was correlated primarily with a significant decrease in naïve T cells (Fig. 3B; 1.7 vs. 3.4×10^5 cells/spleen in SKH1 vs. B6 mice, p=0.008) and memory T cells (Fig. 3B; 1.4 vs. 0.13×10^6 cells/spleen in SKH1 vs. B6 mice, p=0.008). CD25+ regulatory T cell numbers were also mildly reduced (Fig 3B; 6.0 vs. 4.7×10^5 cells/spleen in SKH1 vs. B6 mice, p=0.04), consistent with the mild reduction in peripheral lymphocytes seen in complete blood counts. Despite these changes in peripheral T cell numbers and subset distribution, lymph node cell *in vitro* proliferative response to antigen re-challenge (KLH) was preserved (Fig. 3C). Likewise, positive control responses to anti-CD3 stimulation were similar to B6, with SKH1 exhibiting a significant increase even compared to B6 (Fig. 3C).

To verify that the *in vitro* T cell-dependent immune response correlated to *in vivo* immune functions, a delayed-type hypersensitivity assay was performed using KLH, the same antigen used for the *in vitro* tests. Inflammatory response to KLH following initial sensitization and subsequent challenge did not differ significantly between the SKH1 and B6 mice (Figure 3D).

Tumor histology for tumor-bearing GEMM mice with or without *hr* mutations is comparable

In order to evaluate dendritic cell function in tumor-bearing mice harboring homozygous SKH1 mutations ($Hr^{SKH1/SKH1}$), we performed histology and immunohistochemistry on tumors from $Myf6^{ICNm/WT}$ $Pax3^{P3Fm/P3Fm}$ $Trp53^{F2\text{-}10/F2\text{-}10}$ $Rosa26^{Lusapm/WT}$ mice harboring wildtype *Hr* alleles or homozygous SKH1 mutation (Fig. 4). The tumors were essentially indistinguishable at the histological level between the two groups. The tumors in both groups were composed of sheets of epithelioid cells arranged in nests and sheets. The lesional cells had enlarged, rounded or polygonal nuclei with clumpy chromatin and variably prominent nucleoli. There was significant nuclear pleomorphism and variable numbers of larger cells with more abundant cytoplasm consistent with rhabdomyoblasts. Mitotic activity including atypical mitotic figures was brisk. Histological and immunohistochemical features of myogenin positivity were unchanged by the presence of homozygous SKH1 mutation (n=4 per cohort; representative results are given in Fig. 4A to B). Both cohorts of mice had varying degrees of tumor-associated necrosis that influenced the degree of CD56+ NK cell or CD163+ macrophage infiltration (Fig. 4C to D). The range for the maximum number of CD56+ positive cells seen per tumor in a non-necrotic field of view was 3–189 vs. 13–276 for SKH1 vs. control, respectively (the rhabdomyosarcoma control animals are on a mixed background of C57Bl/6 and SV/J129). Similarly, for CD163+ cells the range was 12–99 vs. 64–101 for SKH1 vs. control, respectively. Thus, the presence or absence of CD56+NK cells and CD163+ macrophages in tumors was unaffected by SKH1 mutation. Tumor growth rates were also indistinguishable between mice bearing alveolar rhabdomyosarcoma tumors whether these mice carried 0 or 2 SKH1 mutations at the *Hr* locus ((p=0.95; Supplementary Figure S2). Tumors in mice homozygous for SKH1 mutations were often also easier to monitor as a result of furlessness.

The SKH1 mouse line allows multiplex optical imaging

As proof of principal that interbreeding homozygous SKH1 mutation into a genetically-engineered model can improve optical imaging of tumor-bearing mice, multiplex imaging was performed to detect viable rhabdomyosarcoma tumor cells from a luciferase allele ($Rosa26^{Lusapm}$) while concurrently examining capillary leak using IR-820 (2) and matrix metalloprotease activity in the same animal (Fig. 5A to B). Viable tumor cells were seen at the periphery of the tumor, as well as at an ectopic site in the left upper quadrant (Fig. 5A to B, panels second from left, arrows). Capillary leak was seen throughout the left lower limb (Fig. 5A to B, panels second from right), but matrix metalloprotease activity was seen only in the tumor's proximally advancing edge at the ankle (Fig. 5A to B, rightmost panels, arrows). Abdominal MMPsense signal in the abdomen was attributed to alfalfa-containing mouse chow (Supplementary Figure S3). At necropsy, the metastatic lesion was determined to be a lymph node (Fig. 5C), and the primary tumor and lymph node metastasis were both histopathologically diagnosed as alveolar rhabdomyosarcoma (Fig. 5D to I).

Discussion

In our studies we have presented an immunological evaluation of the $Hairless^{SKH1/SKH1}$ mouse (SKH1 strain) in comparison to C57Bl/6 controls. In the current outbred state of the SKH1 strain, overall blood leukocyte counts and differential were essentially similar to C57Bl/6. In the evaluation of humoral immunity, a consistent but mild decrease in pre- and

post-immunization IgM levels was found in SKH1 mice, but post-immunization IgG levels were the equivalent to C57Bl/6. The evaluation of cellular immunity revealed statistically significant modest differences in several lymphocyte subsets, but, importantly, a functional proliferation assay of immunized lymphatic cells re-stimulated with a foreign antigen *ex vivo* was as robust for SKH1 mice as C57Bl/6 mice. When homozygosity for the *Hairless*^{SKH1} mutation was interbred to a conditional, genetically-engineered mouse model of alveolar rhabdomyosarcoma, the degree of macrophage and natural killer cell infiltrates were not altered. In addition, tumor phenotype (histology and tumor growth rate) was unchanged. Thus, the *Hairless*^{SKH1} mutation represents a heritable, easily genotyped fur-free phenotypic trait that does not significantly alter immune function for preclinical disease models. Furthermore, the fur-free nature of genetically-engineered mice harboring homozygous *Hairless*^{SKH1} mutation is especially amenable to multiplex optical imaging that can analyze tumor extent, capillary integrity and biochemical (enzymatic) activity *in vivo* concurrently and/or serially.

The SKH1 mouse represents one of a spectrum of hypomorphic (mild), autosomal recessive mutations in the *Hr* gene that nevertheless result in alopecia (recently reviewed in (17)). Mice with severe mutations in the *Hairless* gene are designated *Rhino* (also called, *hrrh*). A targeted *null* allele of *Hairless* is very similar to *Rhino* (5). Historically, humoral and cellular immunity evaluations of *Hairless* mice were performed as early as 1974 (18–20); however, a contemporary evaluation of the SKH1 strain in its current outbred state has not been performed. Here, we establish the SKH1 strain to be functionally immune competent in its current outbred state.

Reports dating back to 1969 suggest an increased incidence of T cell leukemia in 8–10 month old *hr/*hr mice (21,22), which has been attributed to cooperativity with other endogenous viruses (21–23), but not reactivation of *pmv43* since the integrated provirus would not be expected to itself reactivate. However, in a commercially operated isolator-based breeding colony of more than 500 breeders, observed daily and routinely kept to approximately 6–8 months of age, no mice with lymphoproliferative neoplasia have been found in the last 5 years (CB Clifford, personal communications). This dramatic difference in the rate of hematopoetic cancer may reflect either a change in the endogenous (retroviral) burden over time, or that environmental factors in the past led to more lymphoma than is now present. Mouse colony environments are now more controlled than in the past, and thus infectious and non-infectious causes of chronic inflammation are fewer, which we speculate could influence the rates of lymphoma in predisposed strains. The improved ability to discern lymphoma from reactive lymphoid proliferation due to infectious causes (*e.g.*, Myclopasma) is another possible contributor to the differences in apparent lymphoma rates over time. However, a genetic predisposition to leukemia may nonetheless be present, given that homozygous *hr* mice historically develop leukemias at much higher incidences than heterozygous *hr* mice or wildtype mice (21–23). Knowing if or how the *Hairless* gene functions as a tumor suppressor in the hematopoetic lineage remains an interesting future topicof study. Whether a *Hairless* mutation would confound each specific genetically-engineered mouse model of human cancer would need to be investigated on a case by case basis. In the case of rhabdomyosarcoma, the biology of tumors appears essentially unchanged in the cohorts that we examined. And while the role of Hairless (a nuclear receptor co-repressor) is becoming increasingly well characterized at the molecular level (5,24), the role of Hairless as a tumor initiating mutation in the absence of a secondary carcinogen is less obvious in mouse or man ((OMIM 602302) and reference (11)). However from an experimental point of view, fortunately, the proviral integration would be expected to be stable; although the *pmv43* integration into the *Hr* locus was first discovered by a rare revertant resulting from recombination of the LTRs (1), the rate of reversion of MuLV

proviruses has been shown to be very low in examples such as the d^v coat color insertional mutation in DBA mice (a somatic reversion rate of 9×10^{-7} events per animal (25)).

The driving purpose of this immunological evaluation of the SKH1 mouse strain was to characterize a furlessness trait that does not interfere with immune competence but could be genotyped and interbred to genetically-engineered mouse models of human cancer so that optical imaging could be improved. As stated earlier, fur reduces luminescent and fluorescent reporter gene signal by more than 10 fold (3). Heritable furlessness would have utility in both academic medicine and the pharmaceutical industry where preclinical therapeutic studies using genetically-engineered mice are of increasing importance. The alternative use of depilatory agents is time-intensive, can be associated with hypothermia, and often leads to hyperpigmented macules that themselves attenuate fluorescent or luminescent signal emanating from tumors (unpublished data). The C57Bl/6J-Tyr$^{c\text{-}2J}$/J mouse strain, which carries an autosomal recessive *Tyrosinase* (*Tyr*) mutation, provides another alternative to SKH1 mice, in that C57Bl/6J-Tyr$^{c\text{-}2J}$/J mice are albino and their fur is unpigmented (26). Use of C57Bl/6J-Tyr$^{c\text{-}2J}$/J mice carries a different set of considerations, in that these mice undergo retinal degeneration (27) and their use does not necessarily overcome the entirety of reporter gene signal attenuation or scatter associated with fur.

Thus, the SKH1 mouse line presents one very practical approach to improved optical imaging ingenetically -engineered mice without sacrificing immune competence. We believe the SKH1 mouse line will be of significant value to cancer research. We recognize that the use of *Hairless* mutation mice for small animal optical imaging is already extending to fields outside oncology (28,29), and we hope that this contemporary immunological evaluation will extend use of the SKH1 immunocompetent, fur-free mouse strain for a multitude of preclinical cancer studies using GEMMs.

Supplementary Material

Refer to Web version on PubMed Central for supplementary material.

Acknowledgments

Funding for this investigator-initiated study was provided in part from Charles River Laboratories and 5R01CA133229-02 to CK. CK is a member of the Cancer Therapy Research Center (2P30CA054174-17). We thank Dr. Thom Saunders, Dr. John Sundberg, Dr. John Coffin and Dr. Jonathan Stoye for advice in these studies and Lee Ann Zarzabal for statistical support.

Abbreviations

Hr	*Hairless gene*
GEMMs	genetically-engineered mouse models

References

1. Stoye JP, Fenner S, Greenoak GE, Moran C, Coffin JM. Role of endogenous retroviruses as mutagens: the hairless mutation of mice. Cell 1988;54:383–91. [PubMed: 2840205]
2. Prajapati SI, Martinez CO, Bahadur AN, et al. Near-infrared imaging of injured tissue in living subjects using IR-820. Mol Imaging 2009;8:45–54. [PubMed: 19344575]
3. Nishijo K, Hosoyama T, Bjornson CR, et al. Biomarker system for studying muscle, stem cells, and cancer in vivo. FASEB J 2009;23:2681–90. [PubMed: 19332644]
4. Vintersten K, Monetti C, Gertsenstein M, et al. Mouse in red: red fluorescent protein expression in mouse ES cells, embryos, and adult animals. Genesis 2004;40:241–6. [PubMed: 15593332]

5. Zarach JM, Beaudoin GM 3rd, Coulombe PA, Thompson CC. The co-repressor hairless has a role in epithelial cell differentiation in the skin. Development 2004;131:4189–200. [PubMed: 15280217]
6. Cunliffe VT, Furley AJ, Keenan D. Complete rescue of the nude mutant phenotype by a wild-type Foxn1 transgene. Mamm Genome 2002;13:245–52. [PubMed: 12016512]
7. Brooke HC. Hairless mice. J Hered 1926:17.
8. Cachon-Gonzalez MB, Fenner S, Coffin JM, Moran C, Best S, Stoye JP. Structure and expression of the hairless gene of mice. Proc Natl Acad Sci U S A 1994;91:7717–21. [PubMed: 8052649]
9. Cachon-Gonzalez MB, San-Jose I, Cano A, et al. The hairless gene of the mouse: relationship of phenotypic effects with expression profile and genotype. Dev Dyn 1999;216:113–26. [PubMed: 10536052]
10. Stoye JP, Coffin JM. The four classes of endogenous murine leukemia virus: structural relationships and potential for recombination. J Virol 1987;61:2659–69. [PubMed: 3039159]
11. Panteleyev AA, Paus R, Ahmad W, Sundberg JP, Christiano AM. Molecular and functional aspects of the hairless (hr) gene in laboratory rodents and humans. Exp Dermatol 1998;7:249–67. [PubMed: 9832313]
12. Keller C, Arenkiel BR, Coffin CM, El-Bardeesy N, DePinho RA, Capecchi MR. Alveolar rhabdomyosarcomas in conditional Pax3:Fkhr mice: cooperativity of Ink4a/ARF and Trp53 loss of function. Genes Dev 2004;18:2614–26. [PubMed: 15489287]
13. Keller C, Hansen MS, Coffin CM, Capecchi MR. Pax3:Fkhr interferes with embryonic Pax3 and Pax7 function: implications for alveolar rhabdomyosarcoma cell of origin. Genes Dev 2004;18:2608–13. [PubMed: 15520281]
14. Nishijo K, Chen QR, Zhang L, et al. Credentialing a preclinical mouse model of alveolar rhabdomyosarcoma. Cancer Res 2009;69:2902–11. [PubMed: 19339268]
15. Sundberg, JP. The hairless (hr) and rhino (hrrh) mutations, chromosome 14. In: Sundberg, JP., editor. Handbook of mouse mutations with skin and hair abnormalities. Boca Raton, FL: 1994. p. 291-312.
16. Sundberg, JP.; Hogan, ME.; King, LE. Normal biology and aging changes of skin and hair. In: Mohr, U.; Dungworth, DL.; Capen, CC.; Carlton, WW.; Sundberg, JP.; Ward, JM., editors. Pathobiology of the Aging Mouse. Washington, DC: ILSI Press; 1996. p. 301-23.
17. Benavides F, Oberyszyn TM, VanBuskirk AM, Reeve VE, Kusewitt DF. The hairless mouse in skin research. J Dermatol Sci 2009;53:10–8. [PubMed: 18938063]
18. Heiniger HJ, Meier H, Kaliss N, Cherry M, Chen HW, Stoner RD. Hereditary immunodeficiency and leukemogenesis in HRS-J mice. Cancer Res 1974;34:201–11. [PubMed: 4588546]
19. Reske-Kunz AB, Scheid MP, Boyse EA. Disproportion in T-cell subpopulations in immunodeficient mutant hr/hr mice. J Exp Med 1979;149:228–33. [PubMed: 310859]
20. Smith SM, Forbes PD, Linna TJ. Immune responses in nonhaired mice. Int Arch Allergy Appl Immunol 1982;67:254–61. [PubMed: 6977495]
21. Meier H, Myers DD, Huebner RJ. Genetic control by the hr-locus of susceptibility and resistance to leukemia. Proc Natl Acad Sci U S A 1969;63:759–66. [PubMed: 4310515]
22. Heiniger HJ, Huebner RJ, Meier H. Effect of allelic substitutions at the hairless locus on endogenous ecotropic murine leukemia virus titers and leukemogenesis. J Natl Cancer Inst 1976;56:1073–4. [PubMed: 186616]
23. Hackett AJ, Manning JS, Owens RB. In vitro production of murine leukemia virus by cells differing in a single allele. J Natl Cancer Inst 1971;46:1335–42. [PubMed: 4325937]
24. Potter GB, Beaudoin GM 3rd, DeRenzo CL, Zarach JM, Chen SH, Thompson CC. The hairless gene mutated in congenital hair loss disorders encodes a novel nuclear receptor corepressor. Genes Dev 2001;15:2687–701. [PubMed: 11641275]
25. Seperack PK, Strobel MC, Corrow DJ, Jenkins NA, Copeland NG. Somatic and germ-line reverse mutation rates of the retrovirus-induced dilute coat-color mutation of DBA mice. Proc Natl Acad Sci U S A 1988;85:189–92. [PubMed: 3422417]
26. Le Fur N, Kelsall SR, Mintz B. Base substitution at different alternative splice donor sites of the tyrosinase gene in murine albinism. Genomics 1996;37:245–8. [PubMed: 8921397]

27. Bravo-Nuevo A, Walsh N, Stone J. Photoreceptor degeneration and loss of retinal function in the C57BL/6-C2J mouse. Invest Ophthalmol Vis Sci 2004;45:2005–12. [PubMed: 15161869]

28. Collaco AM, Geusz ME. Monitoring immediate-early gene expression through firefly luciferase imaging of HRS/J hairless mice. BMC Physiol 2003;3:8. [PubMed: 12927048]

29. Collaco AM, Rahman S, Dougherty EJ, Williams BB, Geusz ME. Circadian regulation of a viral gene promoter in live transgenic mice expressing firefly luciferase. Mol Imaging Biol 2005;7:342–50. [PubMed: 16240059]

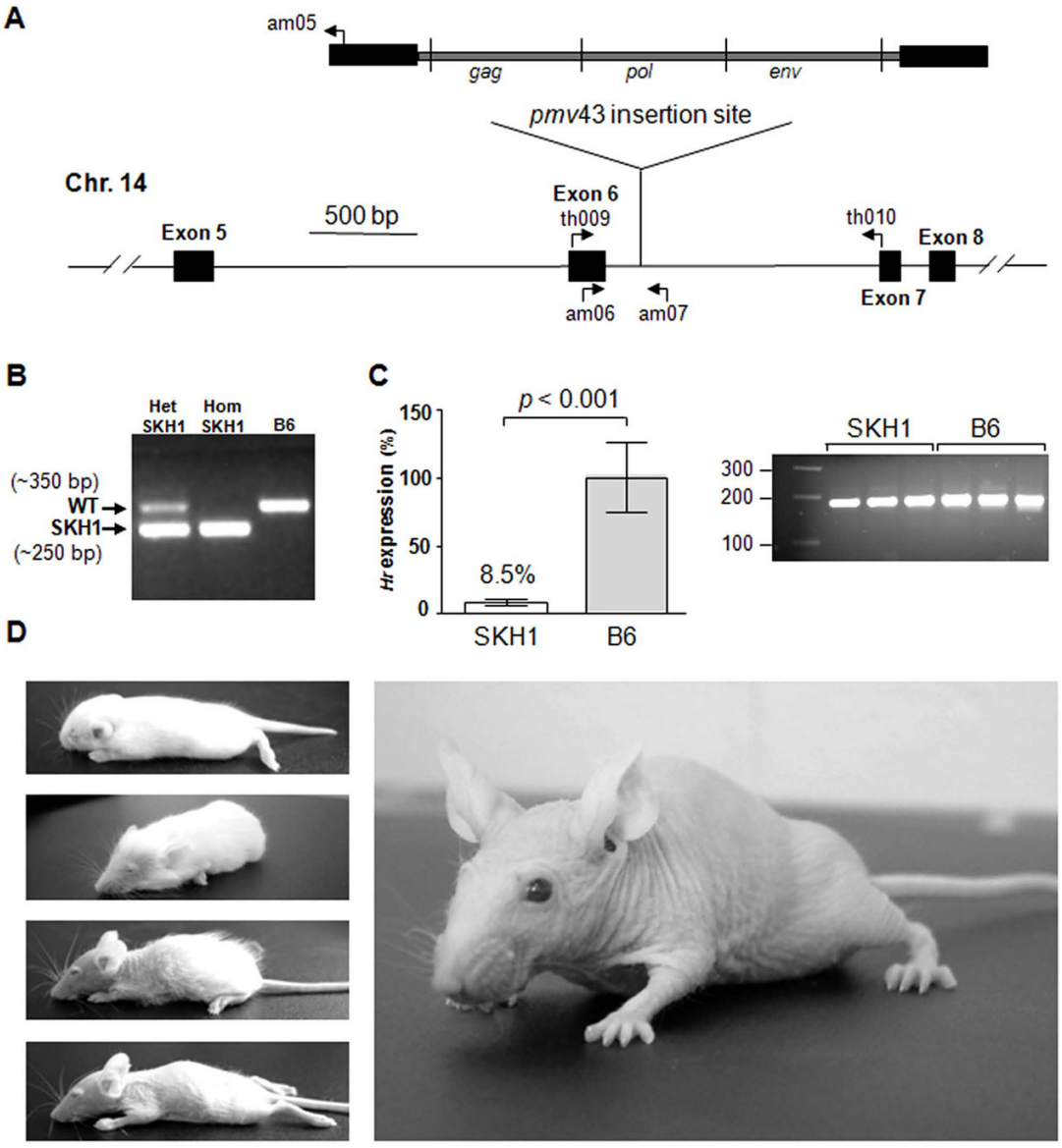

Figure 1. Genetic and Morphological Features of the *Hairless*^{SKH1} Mouse

A, Genomic structure of the *Hairless* gene as related to viral insertion, genotyping primers (am05, am06, am07) and RT-PCR primers (th009 and th010). While *pmv*43 has not been yet sequenced by any group, the size of *pmv*43 is estimated at 9.5 Kb based upon the largest clone (MX40A) having extended 3′ from a BamHI restriction site in *pol* (1), which is then assumed to be approximately 4.1 Kb from the 5′ end of the prototypic *pmv*. Note, also, that labeling of exons given here is consistent with the published literature, but that databases now predict *Hairless* to have 22 instead of 19 exons (Mouse Genome Informatics ID U015825, http://lgsun.grc.nia.nih.gov/geneindex/mm9/bin/giU.cgi?genename=U015825). According to the database schema, *pmv*43 would be inserted between exons 7 and 8, instead of 6 and 7. In this figure, the locus is to scale, but the virus is not to scale. Chr, chromosome. **B,** Genotyping PCR, demonstrating a 350 bp band for wildtype *Hairless* allele and a 250 bp band for the SKH1 allele. Het, herterozygous. Hom, homozygous. **C,** Quantitative RT-PCR showing residual full-length *Hr* transcript in skin of SKH1 mice (left). The PCR product for SKH1 and B6 *Hr* are a singlet band of predicted size. **D,** Progressive rostral to caudal

alopecia in 7, 13, 18 and 24 day old mouse pups (left, top to bottom) as well as a 3 month old adult female SKH1 mouse (right).

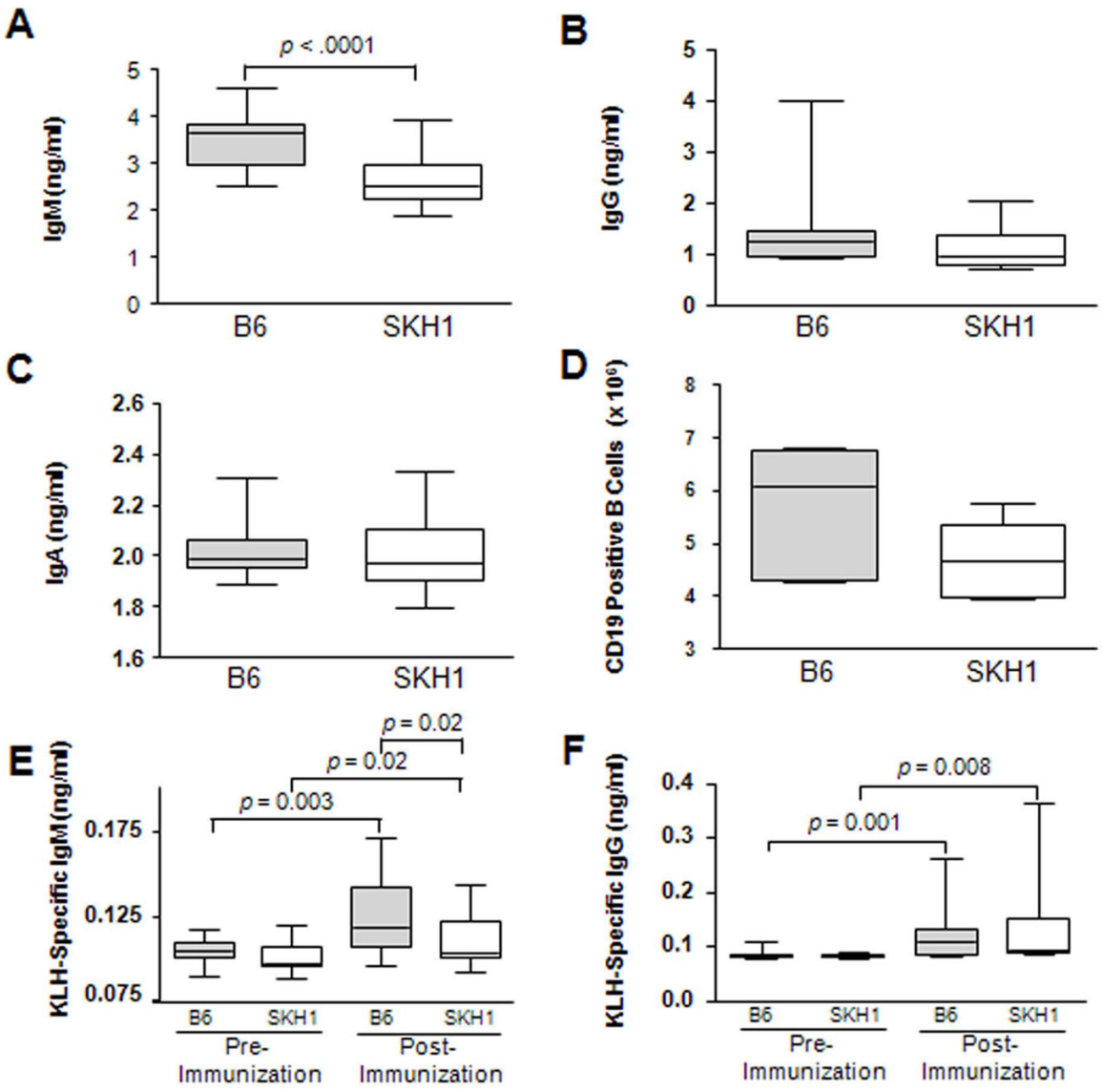

Figure 2. Humoral Immunity of SKH1 vs. B6 mice

A to C, Serum immunoglobin levels of IgM, IgG and IgA, respectively (B6 n=12, 11, 12; SKH1 n=15, 15, 15, respectively). **D,** CD19 positive B cell counts from spleen (B6 n=5; SKH1 n=5). **E to F,** Pre- and Post-immunization anti-KLH antibody IgM and IgG levels, respectively. IgM levels (B6 n=8; SKH1 n=10) were measured 5 days after immunization, and IgG levels (B6 n=11; SKH1 n=10) were measured 2 weeks after immunization.

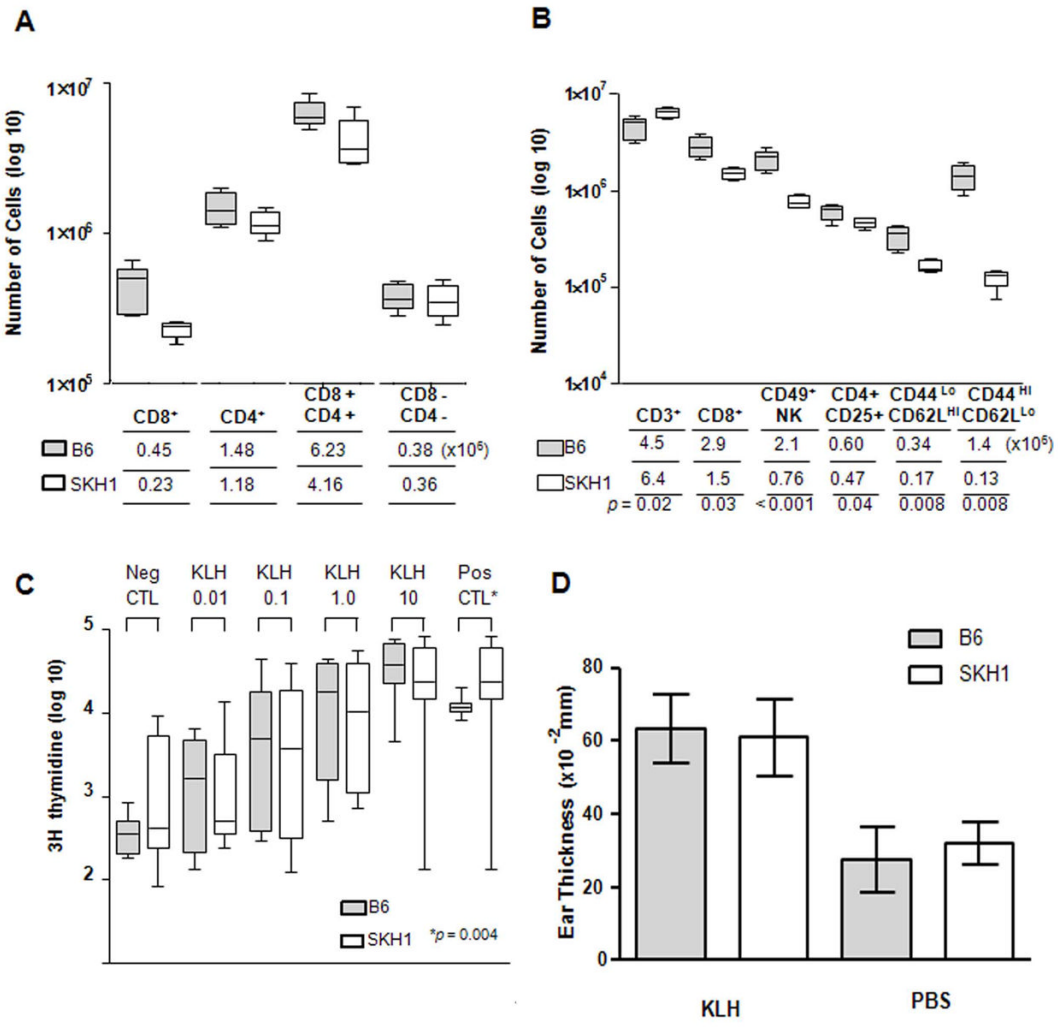

Figure 3. Cellular Immunity of SKH1 vs. B6 mice

A, Thymus cell counts for T cell subpopulations. No statistical differences were found. **B,** Peripheral (splenic) cell counts for CD3 T cells, CD8 T cells, CD49+ Natural Killer (NK) cells, CD4+CD25+ regulatory T cells, $CD44^{Lo}$ $CD62L^{HI}$ naïve T cells and $CD44^{HI}$ $CD62L^{Lo}$ memory T cells. **C,** *ex vivo* leukocyte proliferation following KLH immunization. **D,** *in vivo* immune response following KLH immunization (no significant difference was seen between B6 and SKH1 mice). Data presented in (A) or (B) are absolute numbers of cells per thymus or spleen, respectively. For all experiments, B6 n=5; SKH1 n=5

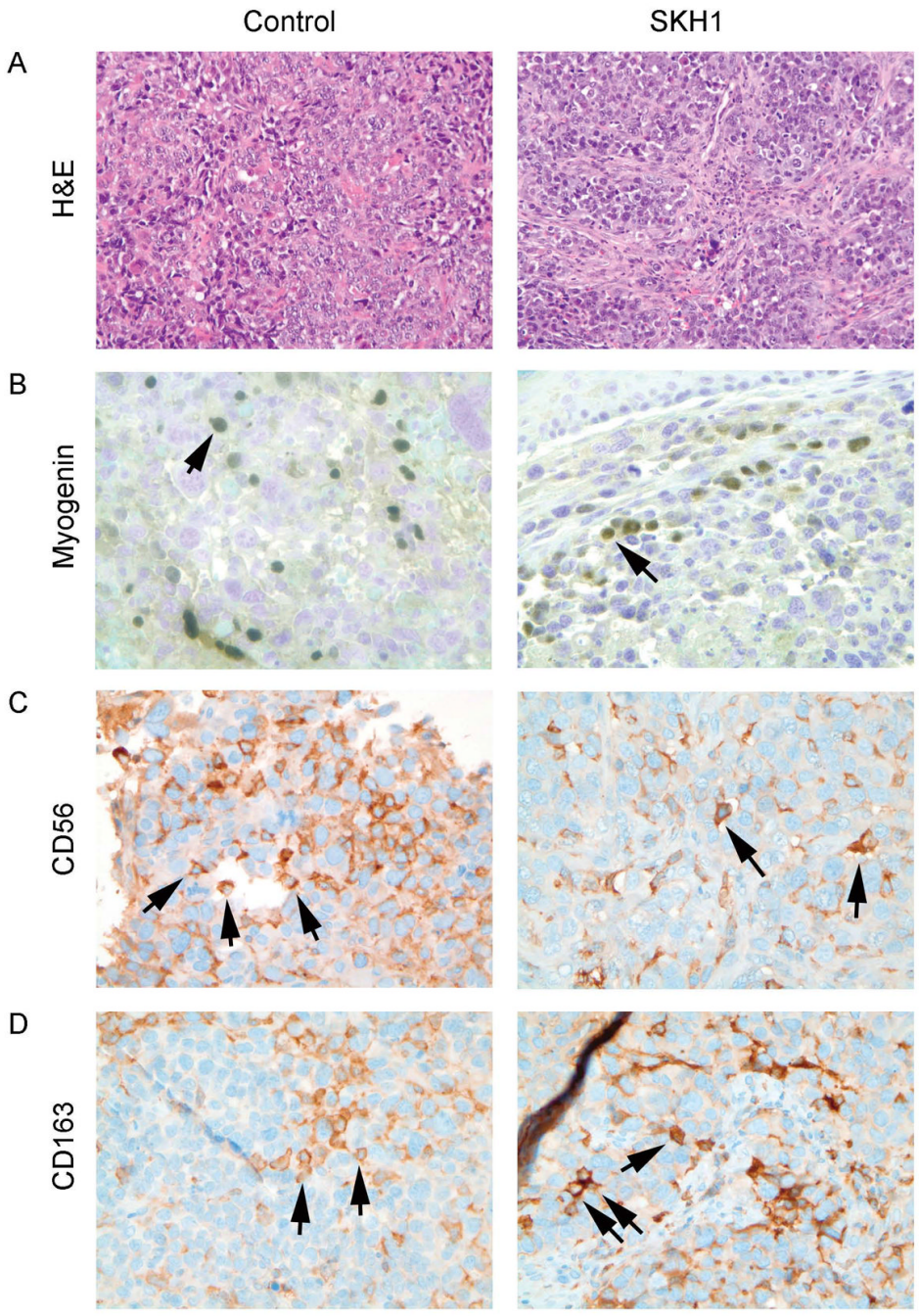

Figure 4. A Hairless Rhabdomyosarcoma Model

A, Histology (Hematoxylin and eosin, H&E) of rhabdomyosarcoma tumors for *Myf6*$^{ICNm/WT}$ *Pax3*$^{P3Fm/P3Fm}$ *Trp53*$^{F2\text{-}10/F2\text{-}10}$ *Rosa26*$^{Lusapm/WT}$ mice harboring wildtype *Hr* alleles (Control, left) or homozygous SKH1 mutation (SKH1, right). **B,** Tumors were positive for myogenin (arrows) in both cohorts. **C to D,** Tumors in both cohorts also harbored infiltrating CD56+ NK cells and CD163+ macrophages, respectively (arrows). All panels represent 400×.

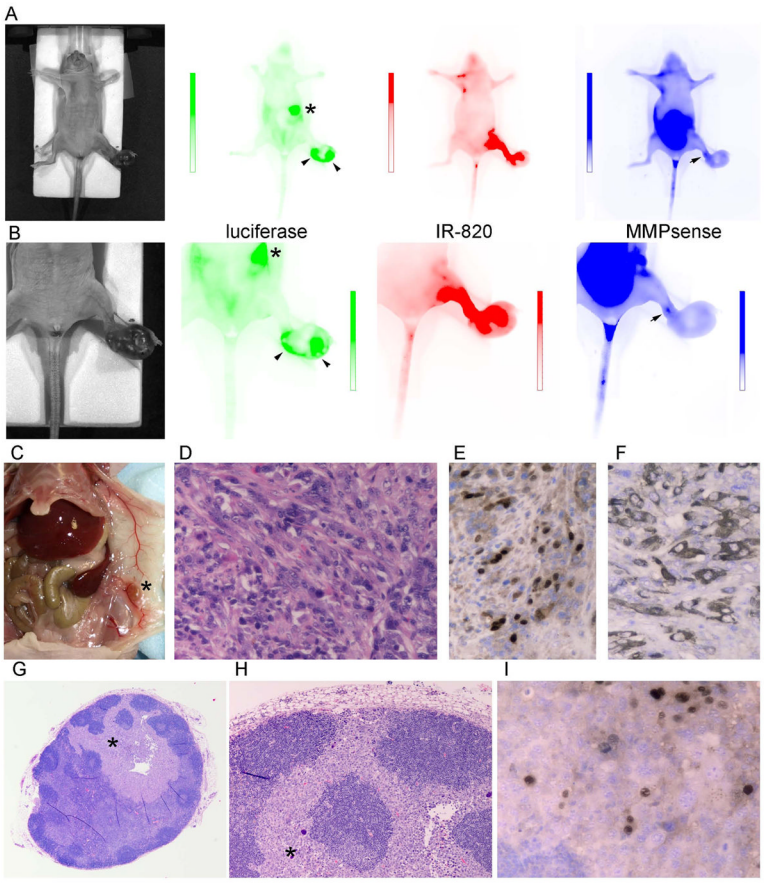

Figure 5. Multiplex Optical Imaging of a Hairless Rhabdomyosarcoma Model

A, From left to right: photograph, luciferase luminescence (scale 2.8×10^5 to 8.0×10^8 p/sec/cm^2/sr), IR-820 fluorescence (scale 3.2×10^5 to 1.6×10^9 p/sec/cm^2/sr) and MMPsense fluorescence (scale 0 to 2.8×10^9 p/sec/cm^2/sr) for a mouse bearing a rhabdomyosarcoma of the left foot. Viable tumor is shown with arrowheads. A metastatic lesion is shown by an asterisk (*). MMPsense activity is shown by an arrow at the advancing front of the tumor. Apparent MMPsense signal in the abdomen is artifact attributable to alfalfa in mouse chow. **B,** repeat imaging for a more restricted field of view. Scales: luminescence (2.8×10^4 to 8.6×10^8 p/sec/cm^2/sr), IR-820 fluorescence (2.1×10^7 to 3.4×10^9 p/sec/cm^2/sr) and MMPsense fluorescence (0 to 4.9×10^9 p/sec/cm^2/sr). **C,** necropsy photomicrograph demonstrating an enlarged subcutaneous lymph node that overlied the spleen. **D,** H&E of primary tumor consistent with rhabdomyosarcoma (400×). **E to F,** Immunohistochemistry positive for nuclear myogenin and cytoplasmic desmin, respectively (400×). **G,** H&E of lymph node shown in A, B and C (20×). **H,** Close-up of G (200×). **I,** Myogenin positive rhabdomyosarcoma cells in the lymph node (400×).

Table 1

Hematological Assessment of *Hairless*$^{SKH1/SKH1}$ Mice. Six mice (3 males and 3 females) ages 160–200 days were evaluated per strain. Statistical approaches are described in the methods section. Values in **bold** indicate indices exhibiting significant differences between C57Bl/6 and Hairless mice.

	C57Bl/6		*Hairless*$^{SKH1/SKH1}$		
	Mean	**Std Dev**	**Mean**	**Std Dev**	***P* value**
White blood cell count (×10^3 cells/μl)	5.04	1.84	7.04	1.28	0.15
Lymphocyte count (×10^3 cells/μl)	4.25	1.71	4.94	1.08	0.52
Monocyte count (×10^3 cells/μl)	0.11	0.07	0.27	0.17	0.11
(% lymphocytes)	**83.20**	**5.22**	**70.12**	**9.47**	**0.05**
(% of monocytes)	2.03	1.20	3.97	2.76	0.3
Red blood cell count (×10^3 cells/μl)	10.89	0.34	10.48	0.38	0.08
Hematocrit	**40.63**	**1.92**	**43.73**	**1.84**	**0.02**
Mean corpuscular volume (fL)	**37.33**	**1.21**	**41.83**	**1.83**	**0.004**
Mean corpuscular hemoglobin (pg)	**14.20**	**0.54**	**15.75**	**0.63**	**0.005**
Mean corpuscular hemoglobin concentration(g/dL)	38.03	1.00	37.73	1.16	1
Red blood cell distribution width (%)	**20.32**	**0.52**	**17.83**	**1.01**	**0.004**
Platelet (×10^3 cells/μl)	414.00	117.13	594.83	277.83	0.26
Mean platelet volume (fL)	6.08	0.12	6.27	0.26	0.25

Mol Cancer Ther. Author manuscript; available in PMC 2011 August 1.